Traffic

Published by John Wiley & Sons Ltd
doi:10.1111/tra.12240

Atg23 and Atg27 Act at the Early Stages of Atg9 Trafficking in *S. cerevisiae*

Steven K. Backues[1,2], Daniel P. Orban[1,3], Amélie Bernard[1], Kushal Singh[1], Yang Cao[1,4,5] and Daniel J. Klionsky[1,4,*]

[1]Life Sciences Institute, University of Michigan, Ann Arbor, MI, USA
[2]Current address: Department of Chemistry, Eastern Michigan University, Ypsilanti, MI, USA
[3]Department of Biology/Chemistry, University of Osnabrueck, Osnabrueck, Germany
[4]Department of Molecular, Cellular and Developmental Biology, University of Michigan, Ann Arbor, MI, USA
[5]Current address: Gallus Biopharmaceuticals, Princeton, NJ, USA
*Corresponding author: Daniel J. Klionsky, klionsky@umich.edu

Abstract

Atg9 is a conserved multipass transmembrane protein with an essential role in autophagy. In *Saccharomyces cerevisiae*, it travels through the secretory pathway to a unique compartment, the Atg9 peripheral structures. These structures are then targeted to the phagophore assembly site (PAS), where they are proposed to help deliver membrane to the forming autophagosome. We used '*in vivo* reconstitution' of this process in a multiple-knockout strain to define four proteins, Atg11, Atg19, Atg23 and Atg27, as the core minimal machinery necessary and sufficient for the trafficking of Atg9 to the PAS. Atg23 and Atg27 function in the formation of the Atg9 peripheral structures. Overexpression of Atg9 can bypass the need for Atg23, suggesting that the amount of Atg9 in each peripheral structure is a critical factor in their targeting to the PAS. In contrast, overexpression of Atg23 or Atg27 interferes with Atg9 trafficking, suggesting that these proteins must be present in the appropriate stoichiometry in order to function properly. These data allow us to resolve existing controversies regarding the role of Atg23 and Atg27, and propose a model that ties together previous observations regarding the role of Atg9 in autophagosome formation.

Keywords autophagy, clustering, Cvt pathway, Golgi, phagophore assembly site, sorting, trafficking

Received 6 August 2014, revised and accepted for publication 7 November 2014, uncorrected manuscript published online 11 November 2014, published online 16 December 2014

Macroautophagy, hereafter referred to as autophagy, is a conserved membrane trafficking pathway that delivers cytoplasmic components to the vacuole/lysosome for degradation. Various forms of selective autophagy target specific cargos such as protein aggregates or excess or damaged organelles for disposal and recycling. In contrast, nonselective autophagy, induced by cellular starvation, delivers bulk cytoplasm for nutrient recycling to prolong cell survival. Both types of autophagy rely on a core set of *au*tophagy- related (Atg) proteins, most of which are conserved across eukaryotes (1).

Autophagy has many links to important human diseases, including cancer, neurodegenerative diseases, infections and autoimmune disorders (2). Because of these health implications, much research is being devoted to understanding the fundamental mechanisms of this process. A major model system used for this research is baker's yeast, *Saccharomyces cerevisiae*. Yeast undergo both starvation-induced bulk autophagy as well as various forms of selective autophagy in growing conditions. The best-studied form of selective autophagy in yeast is the *c*ytoplasm-to-*v*acuole *t*argeting (Cvt) pathway, which delivers specific resident hydrolases such as aminopeptidase I (Ape1) to the vacuole lumen.

Both bulk and selective autophagy begin with the formation of a flat or cup-shaped membrane structure termed a phagophore (3). As the phagophore expands, it begins to envelop its cargo, until it seals into a completed

double-membrane vesicle, termed an autophagosome, with the cargo inside. The completed autophagosome fuses with the vacuole/lysosome, exposing the inner vesicle with its cargo to resident hydrolases (4). In *S. cerevisiae*, the autophagosome is built at a specific perivacuolar site termed the *p*hagophore *a*ssembly *s*ite (PAS). How the membrane that is used to build the phagophore is targeted and delivered to the PAS is largely unknown, and remains one of the most critical questions in the field of autophagy research.

The key to this question is thought to lie in the trafficking of Atg9, which has been proposed to direct the delivery of membrane to the PAS. Atg9 primarily localizes to a unique compartment here referred to as the 'Atg9 peripheral structures', which are thought to be at least one of the proximal sources of membrane used to construct the phagophore. These structures correspond to a post-Golgi compartment, because various Golgi-related mutants perturb Atg9 trafficking (5–7), but they do not show a high percentage of colocalization with any established secretory marker (6). Analysis of their movement dynamics by fluorescence microscopy using Atg9 fused to two tandem copies of the green fluorescent protein (Atg9-2GFP) suggests that these structures are primarily vesicular (8), whereas when examined by electron microscopy with immunogold staining of overexpressed Atg9-GFP they appear as tubular-vesicular clusters (6).

The Atg9 peripheral structures can be trafficked to the PAS to participate in autophagosome formation. In addition, it appears that the peripheral structures can be regenerated by Atg9 that has returned from the PAS once the autophagosome is complete (8,9). The critical role of Atg9 in autophagosome formation and the unique itinerary it follows to and from the PAS are both reasons why it is important to understand Atg9 trafficking. A better understanding of the mechanisms by which the peripheral structures are formed and are targeted to the PAS will advance our knowledge not only about autophagosome formation but also of membrane trafficking in general. For this reason, multiple research groups have been investigating the nature of this trafficking pathway. These efforts, to date, have identified a small handful of proteins that are involved in Atg9 trafficking: Atg11 (10,11), Atg17 (12), Atg23 (13,14), Atg27 (14,15), Trs85 (16–18), Arp2/3 (19) and actin (19) have all been described as playing a role in the anterograde trafficking of Atg9 to the PAS under certain conditions.

Atg11 is a coiled-coil tethering protein that directs Atg9 to the PAS during growing conditions, which is necessary for the function of the Cvt pathway (11,20). Atg11 is an effector of the Rab GTPase Ypt1, which promotes vesicle tethering in various membrane trafficking pathways (18). Ypt1's involvement in autophagy and the Cvt pathway is dependent on a GTPase exchange factor, the critical subunit of which is Trs85 (16,17). Atg9 recruits Trs85 to the peripheral structures, where Trs85 activates Ypt1 (18,21). This activation allows the further recruitment of Atg11, which targets the peripheral structures to the PAS in a process analogous to the vesicle-targeting events seen in other membrane trafficking pathways (18,20).

In contrast to this coherent model that has emerged for Atg11 and Trs85, the role of Atg23 and Atg27 is largely uncharacterized. Atg23 and Atg27 are peripheral and single-pass membrane proteins, respectively, and both form a complex with Atg9 at the peripheral structures and the PAS (14). A recent study (8) reported that when autophagy was induced by treatment with the drug rapamycin, fewer peripheral structures were formed in *atg23*Δ and *atg27*Δ mutants, therefore suggesting that these proteins may be involved in the formation of these structures. This is an intriguing observation, which would place Atg23 and Atg27 upstream of Trs85 and Atg11 in the Atg9 trafficking pathway. However, a defect in peripheral structure formation was not reported in previous papers characterizing the *atg23*Δ and *atg27*Δ mutants (13–15), which instead described these proteins as being required for the movement of Atg9 from the peripheral structures to the PAS. The authors of the recent study note this discrepancy, but do not offer an explanation for it (8), leaving it unclear whether it reflects new insight into the role of Atg23 and Atg27 or is instead something specific to the techniques they used (e.g. something that only occurs in rapamycin treatment conditions).

In this study, we use multiple genetic techniques to resolve this question and extended our understanding of Atg9 trafficking. We first used an *in vivo* add-back system to define a minimal set of Atg proteins necessary for the colocalization of Atg9 with Cvt cargo in growing conditions. Deletion and

overexpression of these minimal components then allowed us to define their epistatic relationships with each other in the Cvt pathway and to propose a comprehensive model of Atg9 trafficking to the PAS.

Results

Determination of a minimal set of components sufficient for Atg9 PAS targeting

At present, 33 Atg proteins have been identified in *S. cerevisiae*. To determine which subset of these proteins were sufficient for Atg9 trafficking, we took advantage of a unique reagent, the *m*ultiple-*k*nock*o*ut (MKO) strain. The MKO strain harbors deletions of 24 different *ATG* genes required for autophagosome formation. The re-addition to this strain of specific genes in various combinations allows the '*in vivo* reconstitution' of autophagy, and the definition of the minimal set of proteins necessary for a specific step (22). To monitor the anterograde trafficking of Atg9, we used native promoter-driven Atg9 tagged with three copies of GFP and quantified its colocalization with red fluorescent protein-tagged precursor Ape1 (prApe1). In wild-type (WT) cells, prApe1 is a specific cargo of the Cvt pathway, and serves as a marker for the PAS. In MKO cells, a true PAS may not be formed due to the absence of the majority of Atg proteins. However, the colocalization of membrane-bound Atg9 with the cytosolic Ape1 complex still represents a major step in PAS formation, and can serve as a proxy for Atg9 anterograde trafficking in this minimal reconstitution system.

Atg9 localized to multiple mobile puncta in both WT and MKO cells (Movies S1 and S2). However, in WT cells, nearly 50% of cytosolic prApe1 dots displayed colocalization with Atg9, whereas in the MKO strain <5% of prApe1 dots had a colocalizing Atg9 punctum, a number that likely represents a nonspecific background of apparent colocalization (Figure 1A,B). The addition of a plasmid containing just four genes – *ATG11*, *ATG19*, *ATG23* and *ATG27* – to the MKO strain was sufficient to increase prApe1 colocalization with Atg9 to approximately half of WT levels (Figure 1A,B). As a control, we also tested a plasmid that contained *ATG11*, *ATG23* and *ATG27* but not *ATG19*, the gene encoding the specific receptor protein that binds prApe1 and Atg11. Addition of this plasmid to the MKO strain did not cause an increase in the percentage of prApe1 dots that colocalized with Atg9 (Figure 1A,B). We then further transformed with plasmids containing various additional subsets of these four genes in our add-back system. These experiments showed that Atg11 and Atg19 were both strictly required to see any increase in colocalization over background (Figure 1C). A small increase in colocalization could be seen when either Atg23 or Atg27 was included together with Atg11 and Atg19, but all four proteins were required to see a major increase in colocalization. Therefore, we concluded that Atg11, Atg19, Atg23 and Atg27 represent a functional minimal Atg9 targeting machinery.

Atg23 and Atg27 are involved in Atg9 peripheral structure formation

Having identified Atg11, Atg19, Atg23 and Atg27 as the core proteins necessary and sufficient for the colocalization of Atg9 and prApe1, we next wanted to use our reconstitution system to address the question of which, if any, of these proteins are necessary for peripheral structure formation and which act downstream in bringing the peripheral structures together with prApe1.

The mobile Atg9 puncta formed in the MKO strain appeared less distinct than those seen in WT cells (Figure 1A, Movies S1 and S2). The addition of Atg23 and Atg27 together changed the appearance of the peripheral Atg9 structures in the MKO strain, making them more distinct and significantly brighter (Figure 1D,E). In contrast, the addition of Atg11 and Atg19 together had no effect (Figure 1D,E), suggesting that Atg23 and Atg27 are specifically involved in peripheral structure formation. Addition of either Atg23 or Atg27 alone had a much smaller effect on peripheral structure appearance and brightness (Figure 1F,G), suggesting that they may cooperatively assist in the formation of the Atg9 peripheral structures.

The Atg9 puncta in the MKO strain, similar to those in the WT, showed limited colocalization with markers of the endoplasmic reticulum (ER), ER exit sites, *cis*-Golgi or mitochondria. However, there was an approximate twofold increase in the percentage of Atg9 puncta associated with the *trans*-Golgi marker Sec7 in the MKO strain (Figure 2). This result suggested that in the absence of the minimal core machinery, Atg9 peripheral structures were still formed; however, there was some delay in Atg9 exit from

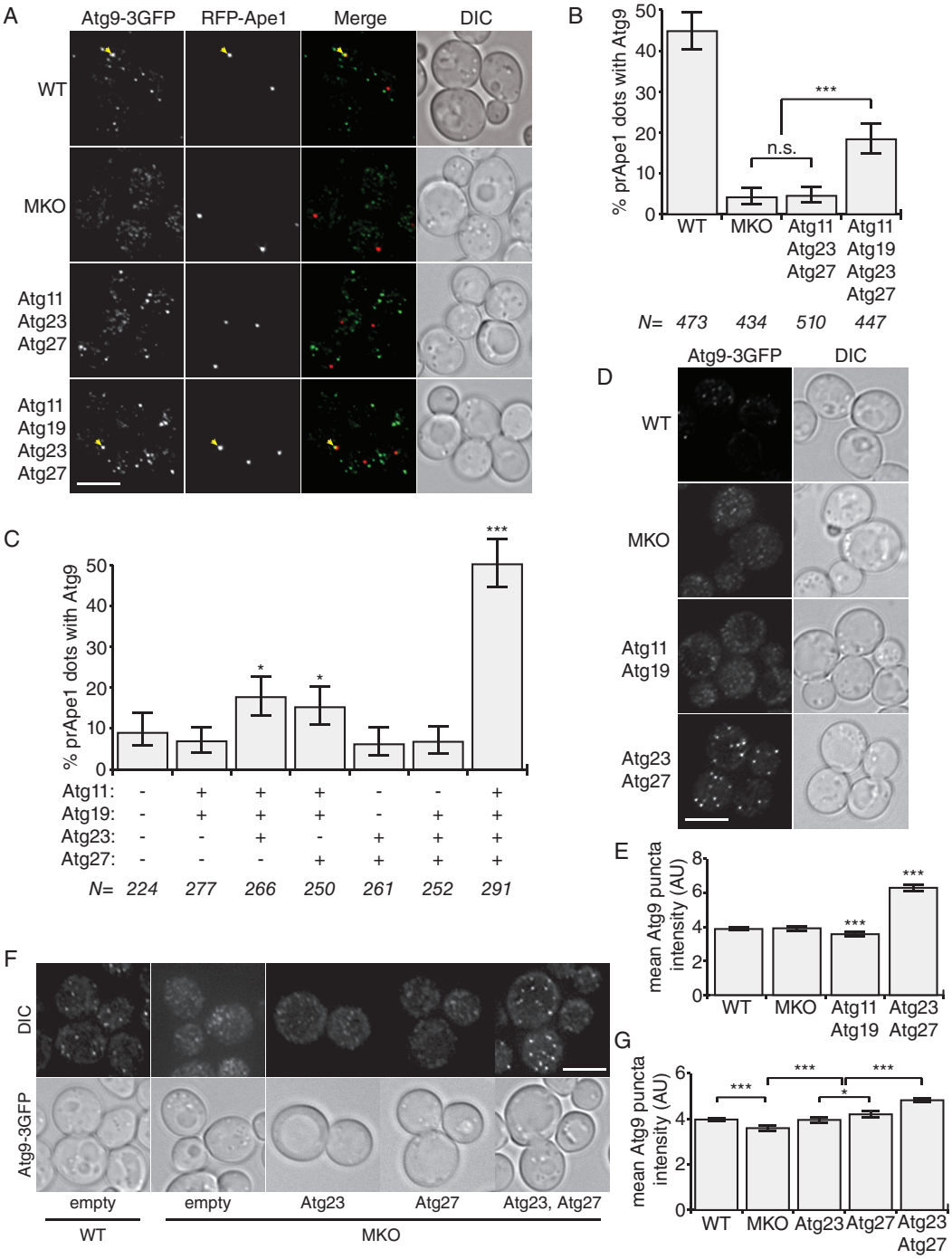

Figure 1: Legend on Next page.

the *trans*-Golgi, and, based on the intensity of the puncta, each structure contained less Atg9. These defects implied that at least some of the minimal core Atg9 trafficking machinery was indeed acting upstream, in peripheral structure formation.

To extend this analysis, we deleted *ATG23* or *ATG27* in a WT background, and compared these to deletions of *ATG11* and *TRS85*. As expected, deletion of any of these four genes caused a loss of Atg9 localization to the PAS (Figure 3A,B). However, in contrast to the *atg11*Δ and

*trs85*Δ strains, the absence of Atg23 or Atg27 caused a major decrease in the brightness of the Atg9 peripheral structures (Figure 3A,C). Endogenous Atg9 protein levels were not affected by the deletion of *ATG23*, *ATG27* or both (Figure 3D), suggesting that the reduced Atg9 fluorescence at the peripheral structures was the result of the mislocalization of Atg9, not a defect in its stability or expression. Consistent with these experiments, deletion of *TRS85* in the MKO strain largely prevented the increased colocalization of Atg9 with prApe1, but not the increased brightness of the Atg9 peripheral structures, seen upon addition of Atg11, Atg19, Atg23 and Atg27 (Figure 3E,F). Together, these data suggest that Atg23 and Atg27 act upstream of Atg11 and Trs85 in Atg9 trafficking during growing conditions.

The interaction of Atg9 with Trs85 and Atg11 is independent of Atg23 and Atg27

Rab proteins and their effectors often act in tethering events; however, Atg11 and Trs85 did not appear to participate in the formation of the Atg9 peripheral structures, suggesting that these components act at a later step of delivery to the PAS. To examine the interaction between these two steps, we first asked whether or not Atg23 and Atg27 or any other Atg proteins were necessary for the known Atg9 – Atg11 interaction using a yeast two-hybrid version of the MKO strain (23). The interaction between Atg11 and the Atg9 N-terminal cytosolic domain was just as robust in the MKO strain as in the WT strain (Figure 4A), suggesting that neither Atg23 nor Atg27 are required for Atg9 to bind Atg11. Next, we determined whether or not Atg23 and Atg27 were necessary for the recruitment of Trs85 to the Atg9 peripheral structures. Trs85-GFP colocalized with Atg9-mCherry in both WT and MKO cells, indicating that Atg23 and Atg27 were also not necessary for this interaction (Figure 4B). Therefore, it appears that neither the recruitment of Trs85 nor the interaction of Atg9 with Atg11 requires Atg23 or Atg27, or any other known Atg proteins. In addition, we found by yeast two-hybrid assay that the interaction between Atg9 and Atg11 was just as robust in a *trs85*Δ strain as in the WT strain, showing that these two proteins bind each other independent of the Atg9 – Trs85 – Ypt1 – Atg11 interaction (Figure 4A). Therefore, it appears likely that Atg9 can recruit Atg11 through two separate pathways, one requiring the recruitment of Trs85 and activation of Ypt1, which then binds Atg11, and the other by direct binding of Atg11 and Atg9.

Overexpression of Atg9 can compensate for the lack of Atg23

As the interaction of Atg9 with both Trs85 and Atg11 appeared to be intact in the absence of Atg23 and Atg27, we next tested whether or not the amount of Atg9 at the peripheral structures is the critical factor in determining the efficiency of their targeting to the PAS. To this end, we made use of Atg9-GFP that was overexpressed under

Figure 1: Definition of the core, minimal Atg9 anterograde movement machinery. A) MKO cells expressing Atg9-3GFP and RFP-Ape1 (SKB227) were transformed with either an empty pRS414 plasmid (MKO) or a pRS414 plasmid containing the indicated *ATG* genes with their native promoters and terminators. These strains along with a WT strain expressing Atg9-3GFP and RFP-Ape1 (SKB170) and containing the empty pRS414 vector were grown in -trp medium, harvested in growing conditions and fixed with formaldehyde to arrest the Atg9 structures prior to imaging. The z-projected images are displayed at equal intensity for comparison. The yellow arrowhead marks an example of colocalized puncta. B) Quantification of the percentage of RFP-Ape1 dots that showed colocalization with Atg9-3GFP was performed automatically. C) MKO cells expressing Atg9-3GFP and RFP-Ape1 (SKB138) containing the indicated *ATG* genes on a combination of pRS414 and pRS416 plasmids (each strain containing both plasmids) were grown in -trp-ura medium, fixed, imaged and quantified as in (B). * = $p < 0.05$ and *** = $p < 0.0001$ versus vector only control. D) MKO (SKB138) cells expressing the indicated *ATG* genes as in (C) were grown along with WT (SKB170) cells expressing empty vectors in -trp-ura medium, fixed, imaged and displayed as in (A). E) Quantification of the mean intensity of Atg9-GFP puncta. F and G) MKO cells expressing Atg9-3GFP (SKB90) and containing the indicated *ATG* genes on pRS414 were grown along with WT cells expressing Atg9-GFP (SKB91) and the empty pRS414 vector in -trp medium, harvested, fixed, imaged and displayed as in (A). G) Quantification of the mean intensity of Atg9-GFP puncta. Scale bars =5 μm. AU, arbitrary intensity units. Error bars =95% CI; * = $p < 0.05$; *** = $p < 0.0001$; n.s. = $p > 0.3$. Note that both the percent colocalization and the average Atg9 puncta intensity were higher when cells were grown in -ura-trp medium (panels C–E) than in -trp medium (panels A, B, F and G).

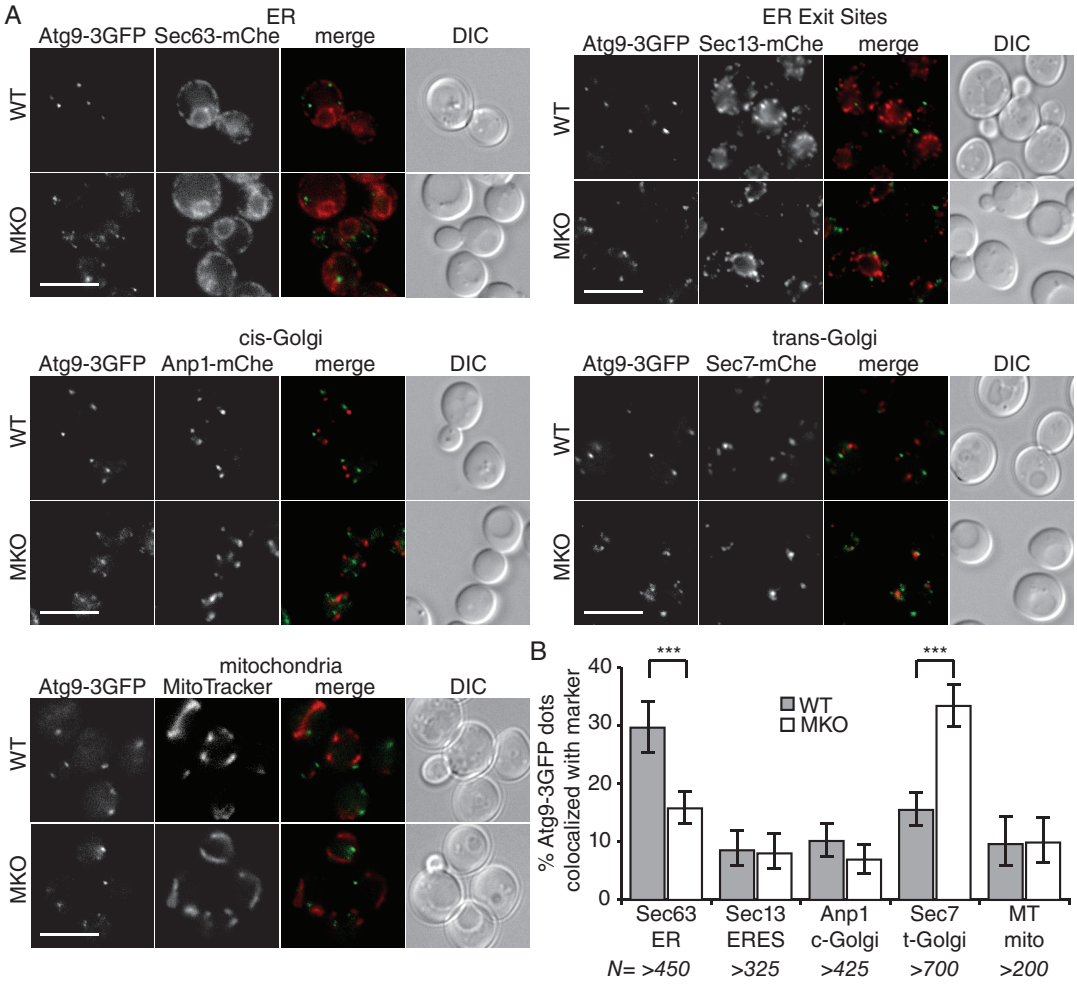

Figure 2: Atg9 in the MKO is partially retained at the *trans*-Golgi, but primarily found in a unique secretory compartment. WT (SKB180, SKB111, SKB181 and SKB182) or MKO (SKB115, SKB221, SKB222 and SKB223) strains expressing native promoter-driven Atg9-3GFP and a secretory marker (Sec63, Sec13, Anp1 or Sec7) chromosomally tagged with mCherry were imaged along with the MitoTracker Red-stained WT (SKB91) or MKO (SKB90) strains expressing Atg9-3GFP alone. A) All images are live cells, single z-plane, with intensity adjusted separately for display; scale bars =5 μm. B) Quantification of colocalization was performed automatically. The indicated markers correspond to the following compartments: Sec63, ER; Sec13, ER exit sites (ERES); Anp1, *cis* (c)-Golgi; Sec7, *trans* (t)-Golgi; MitoTracker Red (MT), mitochondria (mito). Error bars =95% CI; *** = $p < 0.0001$.

the control of the constitutive *TPI1* promoter (6). Overexpressed Atg9-GFP (here referred to as Atg9(OE)) forms brighter peripheral structures with somewhat altered characteristics: namely, they have greatly reduced mobility and showed increased colocalization with Golgi markers (8). However, Atg9(OE) is fully functional in both the Cvt pathway (Figure 5A,B; 6) and nonselective autophagy (6,8).

In order to test the functionality of overexpressed Atg9 in anterograde trafficking to the PAS, we looked at the colocalization of Atg9(OE) with prApe1. We found that approximately 50% of prApe1 dots colocalized with Atg9(OE), slightly more than colocalized with native promoter-driven Atg9 (Figure 5C,D). Unlike native promoter-driven Atg9, Atg9(OE) puncta also frequently colocalized with the *cis*-Golgi marker Anp1-mChe (Figure 5C,E). It was previously suggested that these bright, Golgi-colocalized Atg9 puncta are dead-end structures, and that the functionality of Atg9(OE) in autophagy is due to the additional presence of mobile Atg9 puncta (8).

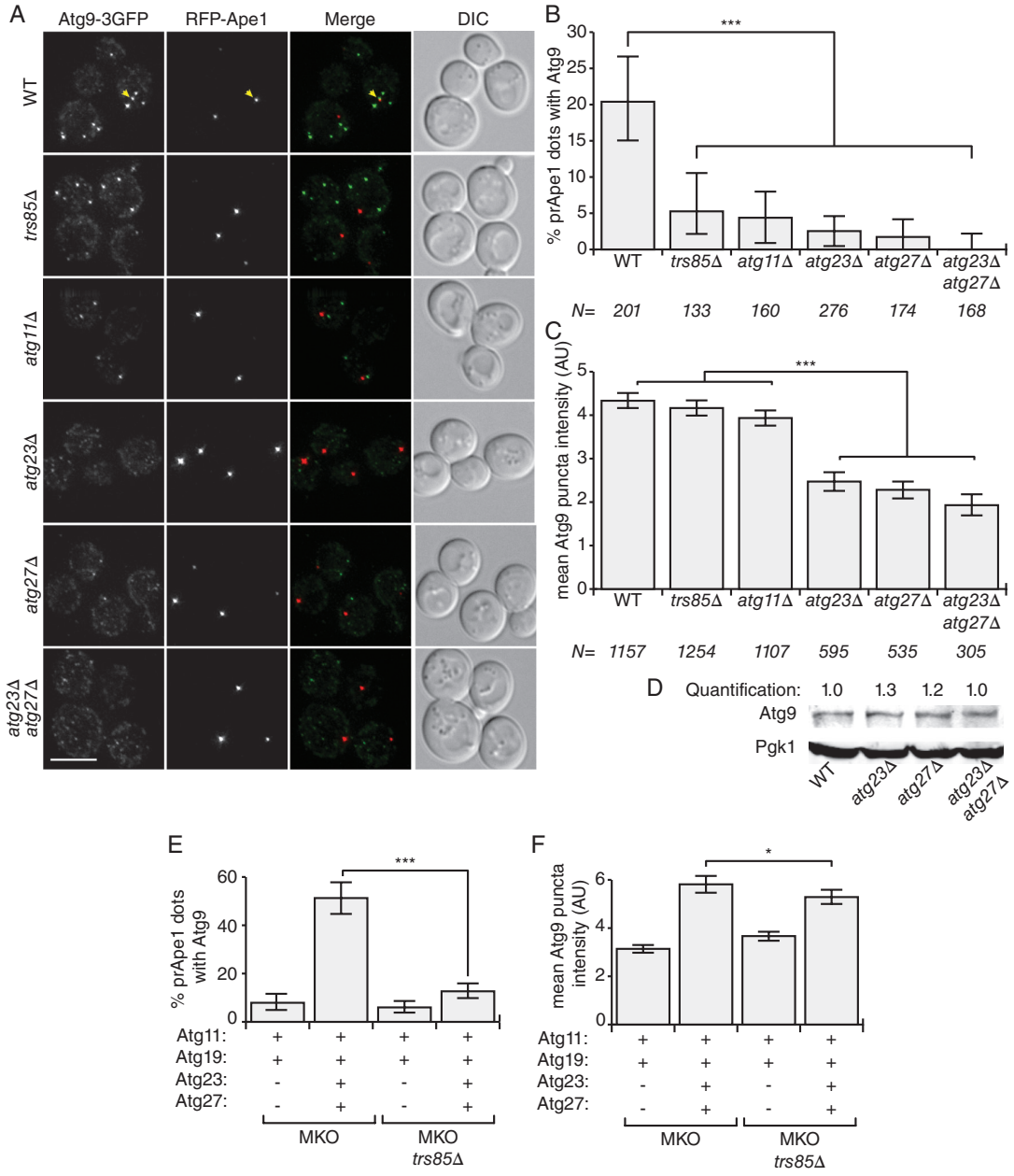

Figure 3: Atg23 and Atg27 affect both PAS targeting of Atg9 and the formation of Atg9 peripheral structures. A) WT (SKB170), *atg11*Δ (SKB220), *trs85*Δ (SKB219), *atg23*Δ (SKB201), *atg27*Δ (SKB202) and *atg23*Δ *atg27*Δ (SKB218) cells expressing native promoter-driven Atg9-3GFP and RFP-Ape1 harvested in growing conditions and imaged after formaldehyde fixation. The z-projected images are displayed at equal intensity for comparison. The yellow arrowhead marks an example of colocalized puncta. Scale bar = 5 μm. B) The percentage of RFP-Ape1 dots that showed colocalization with Atg9-3GFP and (C) the mean intensity of Atg9-3GFP puncta were quantified. D) Atg9 protein levels in WT (WLY176), *atg23*Δ (SKB126), *atg27*Δ (SKB128) and *atg23*Δ *atg27*Δ (SKB130) cells were assessed by western blot with antibodies against Atg9; Pgk1 was used as a loading control. Quantification corresponds to band intensity relative to WT. E and F) MKO (SKB227) and MKO *trs85*Δ (YDO045) cells expressing Atg9-3GFP and RFP-Ape1 and the indicated *ATG* genes on a combination of pRS414 and pRS416 plasmids (each strain containing both plasmids) were grown in -trp-ura media, fixed, imaged and quantified as in (B) and (C). AU, arbitrary intensity units. Error bars =95% CI; * = $p < .05$; *** = $p < 0.0001$.

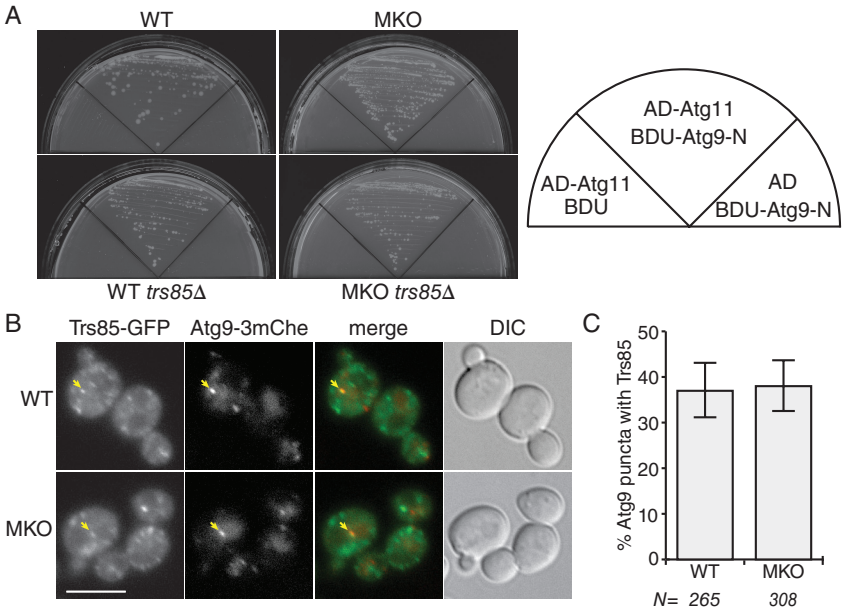

Figure 4: Atg9 and Atg11 interact via two independent routes, and neither requires Atg23 nor Atg27. A) The interaction of Atg11 with the N-terminal part of Atg9 (Atg9-N) is independent of other known Atg proteins and Trs85. WT (PJ69-4A), MKO (YCY148), *trs85*Δ (SKB101) and MKO *trs85*Δ (SKB103) yeast two-hybrid strains were transformed with plasmids expressing AD-Atg11 and BDU-Atg9-N (encoding the cytosolic N-terminal domain). As control, each of these plasmids was also transformed together with an empty BDU or AD plasmid, respectively. The cells were grown for 4 days on selective plates lacking adenine. B) WT (SKB140) and MKO (SKB123) cells expressing Atg9-3mCherry and Trs85-yEGFP were imaged in growing conditions. Images are of live cells, single z-plane, displayed at equal intensity for comparison. Although there appear to be fewer Atg9 puncta in these cells than in the Atg9-3GFP-expressing cells used in other figures, this is likely attributable to the fact that mCherry fluoresces more weakly than GFP. The yellow arrows mark examples of colocalized puncta. Scale bar = 5 μm. C) Manual quantification of the percent of Atg9 puncta that colocalized with a Trs85 puncta. Error bars =95% CI.

However, three-color imaging using Atg9(OE), BFP-Ape1 and Anp1-mCherry showed that Atg9(OE) often colocalized simultaneously with prApe1 and the Golgi (Figure 5C,E), and the Atg9(OE) puncta that colocalized with both markers were not fainter but instead were even brighter than those that colocalized only with the Golgi (Figure 5F). This suggests an alternative explanation, namely that although the peripheral structures formed upon Atg9 overexpression may be somewhat altered, they are still able to recruit prApe1 and carry out selective autophagy. Therefore, we proceeded to determine whether the overexpression of Atg9 could rescue the defect in PAS targeting seen in *atg23*Δ and *atg27*Δ cells.

When Atg9 was expressed at native levels, the deletion of *ATG23* led to the formation of fainter Atg9 puncta that showed little colocalization with prApe1 (Figure 3A–D). In contrast, the puncta formed by Atg9(OE) in *atg23*Δ cells were of equal intensity to those formed in WT cells (Figure 6A–C). The amount of colocalization between the prApe1 and the Atg9-GFP puncta was also the same in both WT and *atg23*Δ strains, suggesting that Atg9 overexpression can compensate for the absence of Atg23 in both the formation of the peripheral structures and their targeting to the PAS (Figure 6A–C). In order to correlate this rescue of colocalization with the overall functionality of the Cvt pathway, we made use of a well-established prApe1 processing assay. The proteolytic cleavage of prApe1 to mature Ape1 occurs only upon delivery of prApe1 to the vacuole by the Cvt pathway (24). In cells expressing native levels of Atg9, the deletion of *ATG23* caused a reduction in the amount of mature Ape1 to undetectable levels. However, in the presence of Atg9(OE), just as much prApe1 was processed in *atg23*Δ as in WT cells (Figure 6D,E).

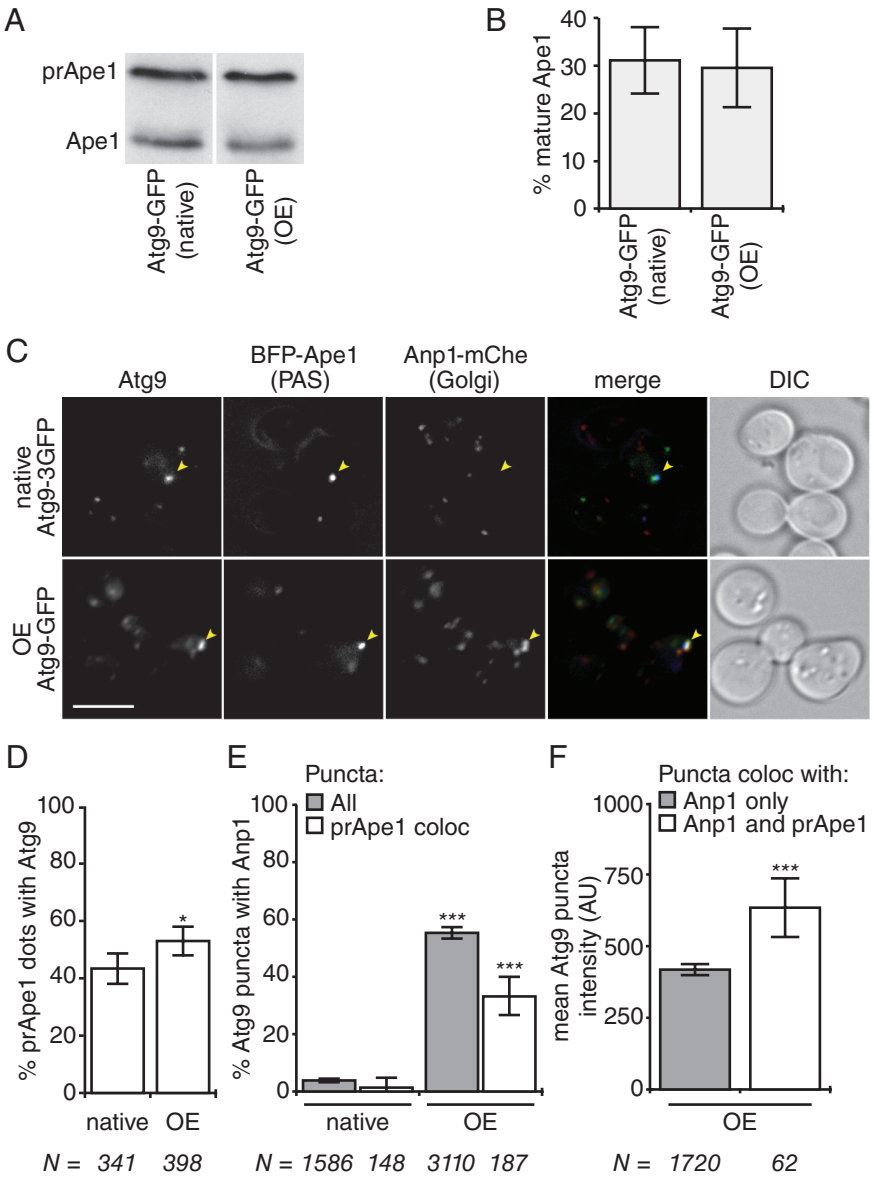

Figure 5: Overexpressed Atg9 colocalizes simultaneously with the *cis*-Golgi marker Anp1 and the PAS marker prApe1**.** A and B) Verification of the functionality of Atg9(OE) in the Cvt pathway. A) WT cells expressing native promoter-driven Atg9-GFP (SKB252) or overexpressing Atg9-GFP from the *TPI1* promoter (SKB134) were harvested in growing conditions and analyzed by western blotting against Ape1. The upper band is unprocessed (cytoplasmic) prApe1, and the lower band is mature (vacuolar) Ape1. Both samples are from a single blot; the white line indicates omitted lanes. B) Quantification of prApe1 processing from four independent blots similar to that shown in (A). C) Single imaging planes of live cells expressing native Atg9-3GFP (YDO046) or overexpressing Atg9-GFP from the *TPI1* promoter (SKB235) in growing conditions are shown. Note that the much brighter intensity of the Atg9(OE) required a shorter exposure time, and so the intensity of the green channels are not directly comparable. The yellow arrows mark examples of colocalized puncta. Scale bar = 5 μm. D) Quantification of the percentage of BFP-Ape1 dots that colocalized with Atg9 and (E) the percentage of Atg9 puncta that colocalized with Anp1-mCherry. Error bars =95% CI; * = $p < .01$; *** = $p < .0001$ versus the corresponding native promoter sample. F) Mean intensity of Atg9(OE) puncta colocalizing with Anp1 only (gray bar) or both Anp1 and prApe1 (white bar) puncta. AU = arbitrary intensity units. Error bars =95% CI; *** = $p < .0001$

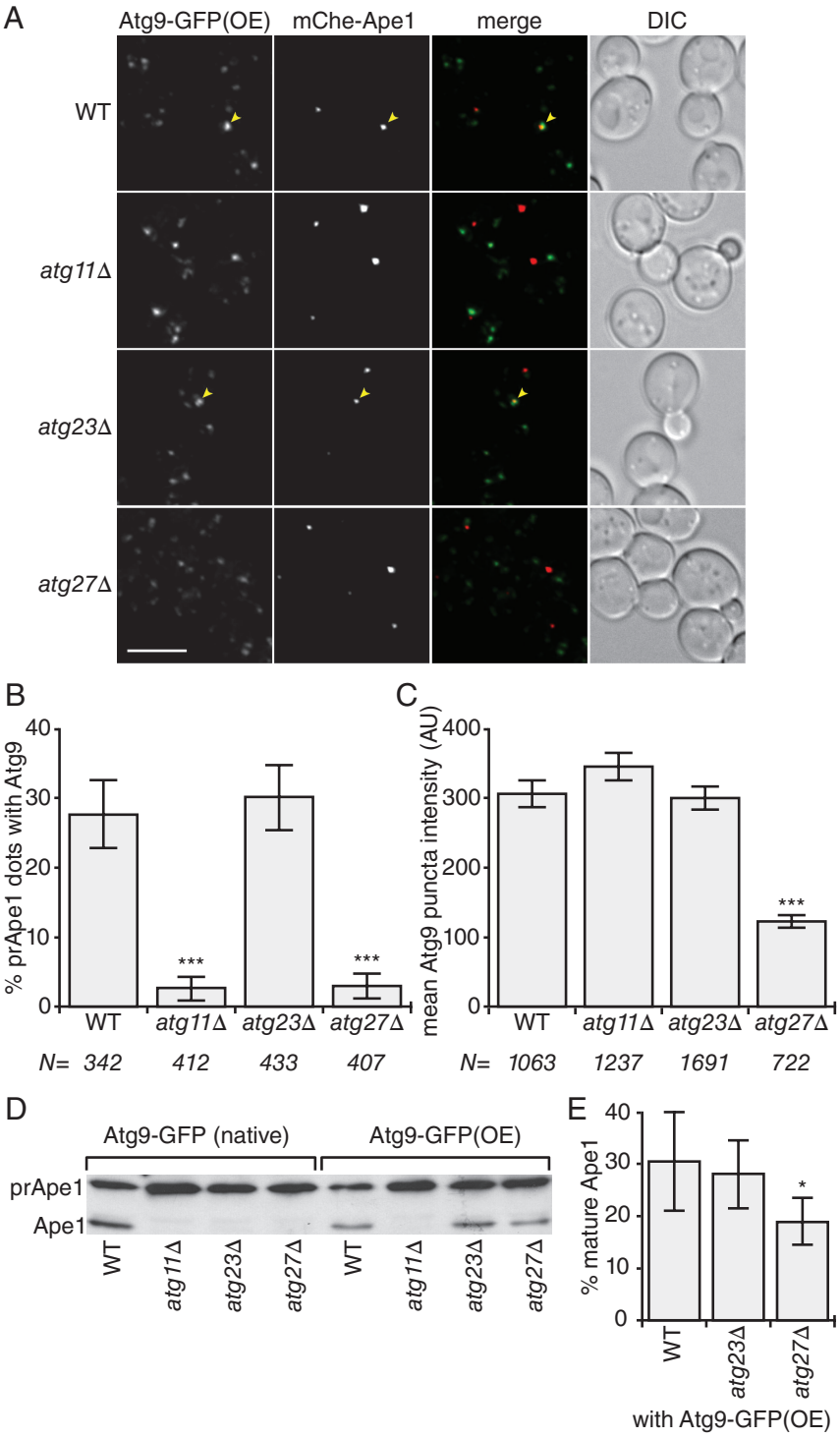

Figure 6: Overexpression of Atg9 can rescue PAS targeting in the *atg23*Δ mutant. A) WT (SKB209), *atg11*Δ (SKB249) *atg23*Δ (SKB247), and *atg27*Δ (SKB248) cells expressing the PAS marker mCherry-Ape1 and overexpressing Atg9-GFP from the *TPI1* promoter were imaged live under growing conditions. Z-projected images, displayed at equal intensity for comparison, are shown. The yellow arrows mark examples of colocalized puncta. Scale bar = 5 μm. B) Quantification of the percentage of RFP-Ape1 dots that colocalized with Atg9-GFP(OE). C) Mean intensity of Atg9-GFP(OE) puncta. D) WT, *atg11*Δ, *atg23*Δ and *atg27*Δ cells expressing native promoter-driven Atg9-GFP (SKB252–SKB255) or overexpressing Atg9-GFP from the *TPI1* promoter (SKB134, SKB250, SKB135 and SKB242) were harvested in growing conditions and analyzed by western blotting against Ape1. The upper band is unprocessed (cytoplasmic) prApe1, and the lower band is mature (vacuolar) Ape1. E) Quantification of the percentage of prApe1 processed into the mature form in WT, *atg23*Δ and *atg27*Δ cells overexpressing Atg9-GFP as in (D); $N = 6$ replicates. AU = arbitrary intensity units. Error bars =95% CI; * = $p < 0.05$ versus WT; *** = $p < 0.0001$ versus WT.

Atg9(OE) in *atg27*Δ cells formed much fainter puncta than in the WT, and showed very little colocalization with prApe1 (Figure 6A–C). Consistent with this finding, there was a partial block in prApe1 processing in the *atg27*Δ strain, even in the presence of Atg9(OE) (Figure 6D,E). Although the defect in colocalization in this case appears more severe than the defect in prApe1 processing, this may simply reflect the fact that the prApe1 processing assay is more sensitive as well as cumulative, and that even though the amount of transient colocalization is too low

to be detectable above background levels by microscopy, it is still sufficient to support partial prApe1 processing.

We also observed a partial mistargeting of Atg9(OE) to the vacuole in the *atg27*Δ strain (our unpublished data), similar to what was reported by Yamamoto et al. (8) for native promoter-driven Atg9.

Therefore, Atg9 overexpression could fully rescue peripheral structure formation, colocalization with prApe1 and delivery of prApe1 to the vacuole in the *atg23*Δ mutant, but not in the *atg27*Δ mutant. In both cases, there was a direct correlation between the amount of Atg9 at the peripheral structures, the efficiency of prApe1 colocalization and the overall functionality of the Cvt pathway. The *atg11*Δ mutant, in contrast, showed a complete block in prApe1 colocalization and processing that was unaffected by Atg9 overexpression (Figure 6) even though it showed no defect in peripheral structure formation (Figure 4). This is further evidence that Atg23 and Atg27 are acting at a distinct step from Atg11 in Atg9 anterograde trafficking. Together, these data support the hypothesis that the amount of Atg9 present in the peripheral structures is a crucial factor for their PAS targeting.

Overexpression of Atg23 or Atg27 inhibits Atg9 trafficking to the PAS

As shown above, overexpression of Atg9 promoted its association with prApe1. As previously reported (11,25), overexpression of Atg11 also promoted trafficking-dependent association of Atg9 and prApe1 (Figure 7A,B). As Atg23 and Atg27 are also positive factors that promote Atg9 PAS trafficking, we wanted to know whether or not overexpression of Atg23 or Atg27 would likewise increase colocalization of Atg9 with prApe1. To test this, we overexpressed Atg23 or Atg27 under the control of the inducible *GAL1* promoter in cells expressing native promoter-driven Atg9-GFP, and measured the brightness of the peripheral structures formed and the colocalization of Atg9 with prApe1. Overexpression of either Atg23 or Atg27 decreased Atg9 puncta intensity and prApe1 colocalization similar to, although generally less severe than, the deletion of either corresponding gene (Figure 7C–F). Similarly, overexpression of either Atg23 or Atg27 led to a partial defect in the Cvt pathway, as measured by the amount of prApe1 that was able to reach the vacuole and undergo proteolytic processing to its mature form (Figure 7G). Therefore, unlike Atg9 or Atg11, Atg23 and Atg27 appear to inhibit trafficking of Atg9 to the PAS when overexpressed, suggesting that a proper stoichiometry of the Atg9–Atg23–Atg27 complex is necessary for the physiological effects of Atg23 and Atg27 in promoting Atg9 anterograde movement.

Discussion

Previous studies addressing the function of Atg23 and Atg27 had reached conflicting conclusions regarding their role in Atg9 trafficking. Multiple earlier studies (14,15) had concluded that, similar to Atg11, they acted in the targeting of the peripheral structures to the PAS. In contrast, a more recent study (8) had indicated that they functioned upstream in the formation of the peripheral structures. Our results allow us to resolve this conflict and propose a model that integrates both sets of observations.

Similar to Yamamoto et al. (8), we found that Atg23 and Atg27 were important for the efficient formation of the Atg9 peripheral structures. This was seen under growing conditions, both with single deletions of the corresponding genes from otherwise WT cells as well as when these proteins were expressed together in MKO cells. While Yamamoto et al. (8) reported the defect in peripheral structure formation as a reduction in the number of peripheral structures, we observed a major decrease in the intensity of Atg9 fluorescence at each peripheral structure, suggesting that less Atg9 was reaching each structure. In *atg23*Δ, *atg27*Δ and *atg23*Δ *atg27*Δ cells, we observed there to be fewer peripheral structures [as reported by Yamamoto et al. (8)] and found that the existing peripheral structures were fainter. MKO cells, in contrast, actually had more peripheral structures than WT cells, although these structures were again much fainter. The addition of Atg23 and Atg27 to the MKO cells caused an increase in the brightness of the peripheral structures, but no increase in their number (our unpublished data). Therefore, the most fundamental role of Atg23 and Atg27 appears to be in controlling the amount of Atg9 in each peripheral structure, presumably by promoting its proper sorting, while the effect on the number of peripheral structures may be secondary or require additional Atg proteins.

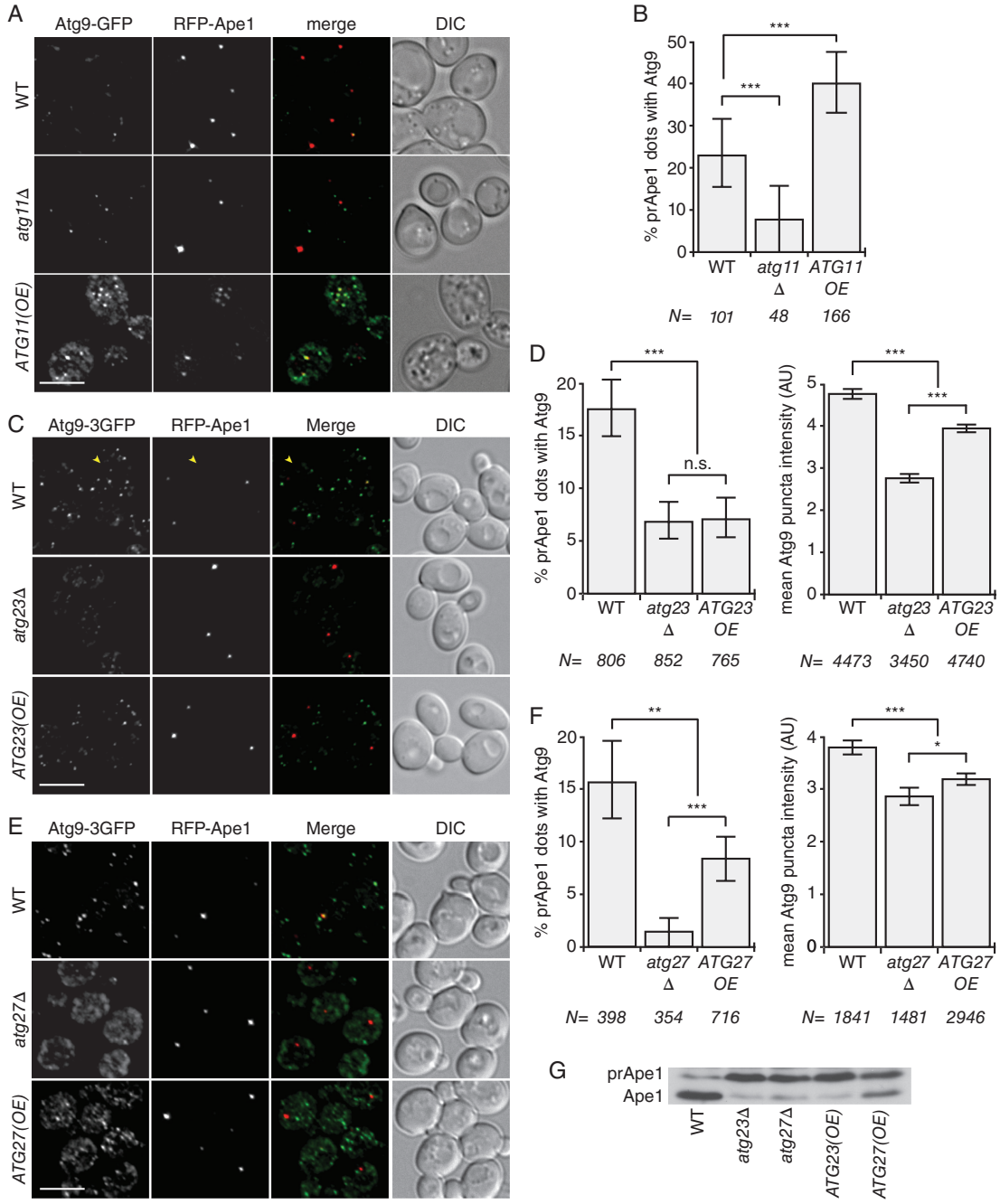

Figure 7: Legend on Next page.

Similar to Legakis et al. (14), we also found that Atg23 and Atg27 were important in the targeting of the Atg9 peripheral structures to the PAS, both in WT cells and in the minimal reconstitution system. While Legakis et al. (14) assessed the efficiency of PAS targeting indirectly by the use of a secondary mutation in *ATG1* (the transport of Atg9 after knocking out ATG1 or 'TAKA assay'), we directly quantified PAS targeting of Atg9 using automated image analysis to determine colocalization of Atg9-GFP with the PAS marker RFP-Ape1. Atg23, Atg27, Atg11, Atg19 and Trs85 were all necessary for efficient targeting of Atg9 to the PAS, but only Atg23 and Atg27 had any effect on the formation of the peripheral structures.

As Atg23 and Atg27 are working both in the formation of the Atg9 peripheral structures and in the targeting of those structures to the PAS, does this mean that they are playing multiple roles at multiple steps of Atg9 targeting? This is a possibility that cannot be excluded; however, a simpler model is that the primary function of Atg23 and Atg27 is in peripheral structure formation, and that inefficient trafficking of Atg9 to the peripheral structures then leads to inefficient targeting of the peripheral structures to the PAS. By this model, the critical factor in determining how efficiently a peripheral structure is targeted to the PAS would be the amount of Atg9 that structure contains, presumably due to the ability of Atg9 to recruit the targeting factors Atg11 and Trs85.

The key piece of evidence supporting this model is the observation that the overexpression of Atg9 can compensate for the absence of Atg23 by artificially increasing the amount of Atg9 present in the peripheral structures. Atg9 overexpression cannot compensate for the lack of Atg11 because Atg11 is the crucial targeting factor that binds Atg9 and brings it to the PAS in growing conditions. Atg9 overexpression can only partially compensate for the lack of Atg27, perhaps because Atg27 has an earlier or more critical role in the integrity of Atg9 transport through the Golgi, so that in the absence of Atg27, overexpressed Atg9 does not overaccumulate in the peripheral structures but is instead partially mistargeted to the vacuole.

As previously reported (11,23), the overexpression of Atg11 promotes Atg9 trafficking to the PAS; this is consistent with our model that the frequency of Atg11 – Atg9 interactions at the peripheral sites is the key factor in the targeting of those peripheral sites to the PAS. In contrast, the overexpression of Atg23 and Atg27 has a dominant negative effect on both peripheral site formation and PAS targeting, suggesting that they are working very differently than Atg11 and that they must form a complex with a defined stoichiometry in order to function properly.

Combining our results with previously published observations allows us to propose an updated model of Atg9 anterograde trafficking (Figure 8). In this model, Atg27 promotes the clustering of Atg9 in specific subdomains of the Golgi, excluding it from mistargeting to the vacuole. Atg23 aids in the further concentration of Atg9 into these subdomains and their release from the Golgi to form the peripheral structures. Atg11 and Trs85 bind to Atg9 in the peripheral structures and target them to the PAS via Atg11's interactions with Atg19, Atg1 and other PAS components.

Recent evidence suggests that the Atg9 peripheral structures are primarily vesicular in nature, although tubular-vesicular clusters may also be formed, perhaps by the action of autophagy-specific SNARE proteins (6,8,26). What could control the budding of these vesicles from the Golgi, and the sorting of Atg9 and Atg27 into them?

A common theme in the packaging of secretory cargo is the formation of specialized subdomains in the *trans*-Golgi where cargo molecules are clustered (26). Both GPI-anchored proteins (27) and the plasma membrane GTPase Pma1 (28) rely on sorting into 'lipid raft' domains for their proper targeting. Pma1 clustering is also

Figure 7: Overexpression of Atg23 or Atg27 interferes with Atg9 trafficking. A) Cells expressing native promoter-driven Atg9-3GFP and RFP-Ape1 (SKB170) and carrying a centromeric plasmid expressing Atg11 from the *CUP1* promoter [ATG11(OE)] or an empty plasmid [WT and *atg11*Δ (SKB220)] were harvested in growing conditions and imaged after formaldehyde fixation. B) The percentage of RFP-Ape1 dots that showed colocalization with Atg9-3GFP and the mean intensity of Atg9-GFP puncta were quantified. C) ATG23(OE) (*GAL1p-ATG23*, SKB198), WT (SKB170) and *atg23*Δ (SKB201) cells were grown in SMG complete (growing conditions for galactose-induced overexpression) and imaged after formaldehyde fixation. D) The percentage of RFP-Ape1 dots that showed colocalization with Atg9-3GFP and the mean intensity of Atg9-GFP puncta were quantified. E and F) ATG27(OE) (*GAL1p-ATG27*, SKB231), WT (SKB170) and *atg27*Δ (SKB202) cells were imaged and quantified as in (C and D). Scale bars = 5 μm. AU = arbitrary units. Error bars = 95% CI; * = $p < 0.05$; ** = $p < 0.001$; *** = $p < 0.0001$; n.s. = $p > 0.3$. G) WT (WLY176), *atg23*Δ (SKB127), *atg27*Δ (SKB129), *GAL1p-ATG23* (SKB196) and *GAL1p-ATG27* (SKB236) cells were grown in YPG (growing conditions for galactose-induced overexpression) and analyzed by western blotting against Ape1. The upper band is unprocessed (cytoplasmic) prApe1, and the lower band is mature (vacuolar) Ape1. This image is representative of two replicates.

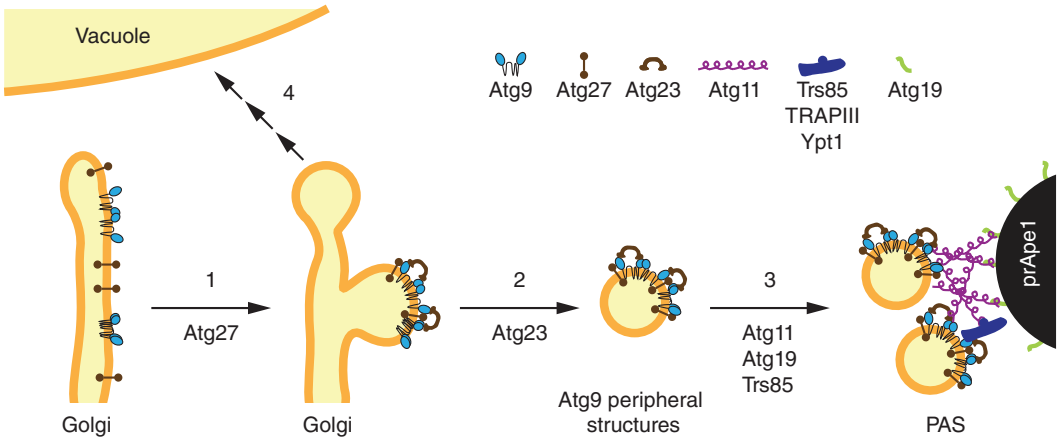

Figure 8: Proposed model of Atg9 trafficking to the PAS. Numbered arrows indicate steps in the Atg9 trafficking pathway. Beneath each arrow is the protein(s) or interaction that facilitates that particular step. Steps are (1) formation of Atg9 clusters within the Golgi, (2) budding of Atg9 clusters to form the Atg9 peripheral sites and (3) targeting of Atg9 peripheral sites to the PAS (shown here is the 'minimal PAS' that was reconstituted in the MKO strain). (4) Normally, Atg9 is excluded from vacuolar transport pathways; however, in the absence of Atg27, the defect in Atg9 clustering may allow some Atg9 to escape its normal trajectory and instead enter into a vacuolar targeting pathway.

aided through crosslinking by a peripheral membrane protein, and mutant Pma1 that fails to cluster is mistargeted to the vacuole (29), similar to Atg9 in the absence of Atg27.

The network of interactions existing among Atg9, Atg27 and Atg23 may likewise work to cluster Atg9 into a specific subdomain of the Golgi that would then become a peripheral structure. The first step would be the formation of Atg9 dimers as a result of its self-interaction (30). An Atg9 mutant that cannot self-interact is severely deficient in the formation of Atg9 peripheral sites, and self-interaction appears to act upstream of other Atg proteins because this mutant is unaffected by the presence or absence of other Atg proteins (our unpublished data). Atg27, whose N and C termini both show interaction with Atg9 (14), might help to collect together Atg9 dimers into larger structures. In the absence of Atg27, the Atg9 dimers might be held less tightly, allowing some to escape into a vacuole transport pathway. Finally, Atg23, which can interact with both the N and the C termini of Atg9, might crosslink Atg9–Atg27 clusters into a larger complex at the *trans*-Golgi, which could then bud into an Atg9 peripheral structure.

Atg9 is conserved in mammals, where it is also trafficked through the secretory pathway to the site of autophagosome formation (31). However, it has not been possible to identify direct mammalian orthologs of Atg11, Atg23 and Atg27 based on sequence similarity (1 and our unpublished data). This may be in part because Atg9 takes a different route through the mammalian secretory system. Indeed, recent reports suggest that mammalian Atg9 first travels to the plasma membrane, and is directed from there via clathrin-mediated endocytosis to a population of recycling endosomes that participate in autophagosome formation (32–34). This is in contrast to the situation in yeast, where clathrin-mediated endocytosis does not appear to play a role in autophagy (26). Nevertheless, even if mammalian Atg9 follows a more complicated itinerary than yeast Atg9, its trafficking still has some of the same fundamental requirements: something must help to sort it into its specific carriers (analogous to the role of Atg23 and Atg27), and something must target those carriers to the site of autophagosome formation (analogous to the role of Atg11). Therefore, even if there are no direct orthologs of Atg11, Atg23 and Atg27 in mammalian cells, it appears likely that there are other mammalian proteins with as-of-yet unidentified roles in Atg9 trafficking that fulfill these functions. The GTPase-activating protein TBC1D5, which colocalizes with mammalian Atg9 and interacts with other components of the autophagic machinery, may be one candidate for an Atg11-like tethering role (35,36), but further studies

will be needed to verify this. Continued work on the fundamental mechanisms of Atg9 trafficking in yeast will serve as an important complement to ongoing investigations in mammalian cells, as better understanding Atg9 trafficking in the yeast system will give insight into what sorts of mammalian proteins might be acting to facilitate ATG9 trafficking.

Materials and methods

Fluorescence microscopy

Cells were grown to mid-log phase before imaging. For colocalization of Atg9-3GFP with RFP-Ape1 and quantification of Atg9-3GFP intensity, cells were fixed for 30 min in 1.5% formaldehyde in wash buffer (50 mM KPO_4 and 1 mM $MgCl_2$), washed once in wash buffer and imaged in wash buffer. All centrifugation steps were 3 min at 1500 × ***g***. To stain the vacuole membrane with FM 4–64, approximately 0.5 OD of log-phase cells were first resuspended in 100 µL of 20 µM FM 4–64 (Life Technologies) and grown at 30°C with shaking for 15 min, then harvested and resuspended in 1 mL of SMD-complete medium and grown for a further 30 min at 30°C with shaking prior to imaging. Staining of mitochondria with MitoTracker Red (Life Technologies) was performed according to the manufacturer's protocol. Images were collected on a Deltavision Elite deconvolution microscope (GE Healthcare/Applied Precision) with a 100× objective and a CCD camera (CoolSnap HQ; Photometrics).

For quantification of Atg9-3GFP and *TPI1* promoter (*TPI1p*)-driven Atg9-GFP puncta brightness and colocalization with RFP-Ape1 or mChe-Ape1, stacks of 20 image planes were collected with a spacing of 0.2 µm to cover the entire yeast cell, and analysis was performed on an average projection of the imaging planes. For colocalization of Atg9-3GFP and *TPI1p*-Atg9-GFP with mCherry-tagged subcellular markers or MitoTracker Red, only a single imaging plane of a living cell was analyzed.

Unless otherwise noted, quantification of fluorescence images was performed automatically using CellProfiler release 2.0.11710 (37). Images were set to equal intensities and saved as TIFFs in ImageJ (38) and then imported into CellProfiler. Green and red fluorescent puncta were identified using the IdentifyPrimaryObjects module. The expected object size, method and threshold correction factor were adjusted independently for each fluorescently tagged protein. We used multiple test images per tagged protein to verify that the objects found by the algorithm matched those that could be visually identified. Once optimal settings for a given tagged protein were found, they were applied consistently across all images containing that tagged protein.

Colocalization was determined using an object-based method. A prApe1 dot was considered colocalized if its center was less than four pixels away from the center of an Atg9 punctum. For colocalization with subcellular markers, an Atg9 punctum was considered colocalized if its center was not more than one pixel away from any portion of the subcellular compartment label. Graphs represent pooled data from at least two imaging sessions on different days.

For nominal data (e.g. percent colocalization), 95% CI was calculated from the binomial distribution using the calculator at http://statpages.org/confint.html, and p values were calculated using Fisher's exact test with the calculator at http://graphpad.com/quickcalcs/contingency1/. For continuous data (e.g. puncta intensity), 95% CI and p values (Student's *t*-test) were calculated in Microsoft Excel®.

General methods and reagents

All yeast media components were from ForMedium. Other chemicals were from Fisher Scientific or Sigma-Aldrich unless otherwise noted. For western blotting, yeast were grown in YPD (1% yeast extract, 2% peptone and 2% glucose) or YPG (1% yeast extract, 2% peptone and 2% galactose) media, as indicated. For microscopy, yeast were typically grown in SMD complete medium (1× yeast nitrogen base, 0.5% casamino acids, 1× complete amino acids and vitamin supplement and 2% glucose). Where indicated, yeast were grown in SMG complete medium (2% galactose instead of glucose) for GAL induction, or SMD-ura-trp medium (1× yeast nitrogen base, 0.5% casamino acids, 1× -ura-trp amino acids and vitamin supplement and 2% glucose) for maintenance of pRS414 and pRS416 plasmids. Quantification of Atg9 protein levels by western blot made use of polyclonal rabbit anti-Atg9 (39) and anti-Pgk1 (a generous gift from Dr Jeremy Thorner, UC Berkley), followed by a fluorescently labeled goat anti-rabbit secondary antibody (IRdye® 800CW; Li-Cor Biosciences), and detection with an Odyssey fluorescence imaging system (Li-Cor Biosciences). *TPI1p*-Atg9-GFP was detected with mouse monoclonal anti-GFP JL-8 (Clontech), and prApe1 processing was detected with rabbit anti-Ape1 (24). These were followed with a horseradish peroxidase-conjugated secondary antibody (Jackson Immunolabs), with chemiluminescent detection using 1:5 diluted Immobilon® western substrate (Millipore) and Blue Basic film (Genemate). Quantification of the scanned film was performed in Adobe Photoshop®.

Plasmid generation

All minipreparations and gel purification were done using PureLink kits from Invitrogen. All enzymes were from New England BioLabs, and all oligonucleotide primers were from Integrated DNA Technologies. LoxP sites were added flanking the *HIS3* gene of pRS303 by two rounds of cloning. In the first round, a 10 µM mixture of the loxP primers ggttATAACTTCGTATAATGTATGCTATACGAAGTTATgggtttacgt and aaacccATAACTTCGTATAGCATACATTATACGAAGTTATaaacccacgt were annealed by heating for 5 min at 95°C and being allowed to cool on the bench. This created a primer dimer with an AatII-compatible overhang. The dimer was then phosphorylated with T4 kinase in 1× ligase buffer according to the manufacturer's protocol. The phosphorylated primer dimer was ligated at a 10:1 insert:vector ratio using T4 ligase into pRS303 that had been linearized with AatII and dephosphorylated with calf intestinal phosphatase. Positive clones of pRS303-loxP(1) were identified by polymerase chain reaction using a primer annealing within

Table 1: List of strains used in this study.

Strain	Genotype	Source
PJ69-4A	*MATa trp1-901 leu2-3,112 ura3-52 his3-200 gal4Δ gal80Δ LYS2::GAL1-HIS3 GAL2-ADE2 met2::GAL7-lacZ*	(44)
PSY253	SEY6210 *atg9Δ::KAN*	This study
SEY6210	MATα *leu2-3,112 ura3-52 his3-Δ200 trp1-Δ901 suc2-Δ9 lys2-801; GAL*	(45)
SKB90	MKO *ATG9-3GFP*	This study
SKB91	SEY6210 *atg9Δ::KAN ATG9-3GFP::URA3*	This study
SKB101	PJ69-4A *trs85Δ::KAN*	This study
SKB103	YCY148 *trs85Δ::KAN*	This study
SKB111	SEY6210 *atg9Δ::KAN ATG9-3GFP::URA3 ANP1-mChe::TRP1*	This study
SKB115	MKO *ATG9-3GFP ANP1-mChe::TRP1*	This study
SKB123	MKO *ATG9-3mChe TRS85-yEGFP::KAN*	This study
SKB126	WLY176 *atg23Δ*	This study
SKB128	WLY176 *atg27Δ*	This study
SKB134	SEY6210 *atg9Δ::KAN TPI1p-ATG9-GFP::URA3*	This study
SKB135	SEY6210 *atg9Δ::KAN TPI1p-ATG9-GFP::URA3 atg23Δ::LEU2*	This study
SKB138	MKO *ATG9-3GFP RFP-APE1::LEU2*	This study
SKB140	SEY6210 *ATG9-3mChe TRS85-yEGFP::KAN*	This study
SKB143	SEY6210 *atg9Δ::KAN TPI1p-ATG9-GFP::URA3 atg23Δ::LEU2 atg27Δ::HIS5 S.p.*	This study
SKB170	SEY6210 *atg9Δ::KAN ATG9-3GFP::URA3 RFP-APE1::LEU2*	This study
SKB180	SEY6210 *atg9Δ::KAN ATG9-3GFP::URA3 SEC63-mChe::TRP1*	This study
SKB181	SEY6210 *atg9Δ::KAN ATG9-3GFP::URA3 SEC13-mChe::TRP1*	This study
SKB182	SEY6210 *atg9Δ::KAN ATG9-3GFP::URA3 SEC7-mChe::TRP1*	This study
SKB196	WLY176 *GAL1-ATG23::HIS3*	This study
SKB198	SEY6210 *atg9Δ::KAN ATG9-3GFP::URA3 RFP-APE1::LEU2 GAL1-ATG23::TRP1*	This study
SKB201	SEY6210 *atg9Δ::KAN atg23Δ ATG9-3GFP::URA3 RFP-APE1::LEU2*	This study
SKB202	SEY6210 *atg9Δ::KAN atg27Δ::HIS5 S.p. ATG9-3GFP::URA3 RFP-APE1::LEU2*	This study
SKB209	SEY6210 *atg9Δ::KAN TPI1p-ATG9-GFP::URA3 mChe-APE1::TRP1*	
SKB218	SEY6210 *atg9Δ::KAN atg23Δ atg27Δ ATG9-3GFP::URA3 RFP-APE1::LEU2*	This study
SKB219	SEY6210 *atg9Δ::KAN trs85Δ::TRP1 ATG9-3GFP::URA3 RFP-APE1::LEU2*	This study
SKB220	SEY6210 *atg9Δ::KAN atg11Δ::HIS3 ATG9-3GFP::URA3 RFP-APE1::LEU2*	This study
SKB221	MKO *ATG9-3GFP SEC63-mChe::KAN*	This study
SKB222	MKO *ATG9-3GFP SEC13-mChe::KAN*	This study
SKB223	MKO *ATG9-3GFP SEC7-mChe::KAN*	This study
SKB227	MKO *ATG9-3GFP RFP-APE1::LEU2 URA3*	This study
SKB231	SEY6210 *atg9Δ::KAN ATG9-3GFP::URA3 RFP-APE1::LEU2 GAL1p-ATG23::HIS3*	This study
SKB235	SEY6210 *atg9Δ::KAN TPI1p-ATG9-GFP::URA3 ANP1-mChe::TRP1 BFP-APE1::LEU2*	This study
SKB236	WLY176 *GAL1p-ATG27::HIS*	This study
SKB238	SEY6210 *atg1Δ::LEU2 TPI1p-ATG9-GFP::URA3*	This study
SKB239	SEY6210 *pep4Δ::LEU2 TPI1p-ATG9-GFP::URA3*	This study
SKB242	SEY6210 *atg9Δ::KAN TPI1p-ATG9-GFP::URA3 atg27Δ::HIS5 S.p.*	This study
SKB243	SEY6210 *atg1Δ::LEU2 TPI1p-ATG9-GFP::URA3 atg27Δ::HIS5 S.p.*	This study
SKB247	SEY6210 *atg9Δ::KAN TPI1p-ATG9-GFP::URA3 mChe-APE1::TRP1 atg23Δ::LEU2*	This study
SKB248	SEY6210 *atg9Δ::KAN TPI1p-ATG9-GFP::URA3 mChe-APE1::TRP1 atg27Δ::HIS5 S.p.*	This study
SKB249	SEY6210 *atg9Δ::KAN TPI1p-ATG9-GFP::URA3 mChe-APE1::TRP1 atg11Δ::HIS5 S.p.*	This study
SKB250	SEY6210 *atg9Δ::KAN TPI1p-ATG9-GFP::URA3 atg11Δ::HIS5 S.p.*	This study
SKB252	SEY6210 *atg9Δ::KAN ATG9-GFP::URA3*	This study
SKB253	SEY6210 *atg9Δ::KAN ATG9-GFP::URA3 atg11Δ::HIS5 S.p.*	This study
SKB254	SEY6210 *atg9Δ::KAN ATG9-GFP::URA3 atg23Δ::LEU2*	This study
SKB255	SEY6210 *atg9Δ::KAN ATG9-GFP::URA3 atg27Δ::HIS5 S.p.*	This study
WLY176	SEY6210 *pho13Δ, pho8Δ60*	(46)
YCY123 (MKO)	SEY6210 *atg1Δ, 2Δ, 3Δ, 4Δ, 5Δ, 6Δ, 7Δ, 8Δ, 9Δ, 10Δ, 11Δ, 12Δ, 13Δ, 14Δ, 16Δ, 17Δ, 18Δ, 19Δ, 20Δ, 21Δ, 23Δ, 24Δ, 27Δ, 29Δ*	(22)
YCY148	MKO *gal4Δ gal80Δ GAL1-HIS3 GAL2-ADE2 met2::GAL7-LacZ*	(23)
YDO045	MKO *trs85Δ::KAN ATG9-3GFP RFP-APE1::LEU2*	This study
YDO046	SEY6210 *atg9Δ::KAN ATG9-3GFP::URA3 ANP1-mChe::TRP1 BFP-APE1::LEU2*	This study

the loxP site, and verified by sequencing over the insert. The second loxP site was added in the same way, except that the primers used were gggtttATAACTTCGTATAATGTATGCTATACGAAGTTATgggttttgca and aaacccATAACTTCGTATAGCATACATTATACGAAGTTATaaaccctgca and the vector was pRS303-loxP(1) digested with *Nsi*I. The ATG9-3GFP fragment was isolated from pRS306-ATG9-3GFP (19) by digestion with *Xho*I and *Sac*I and ligated into *Xho*I/*Sac*I-digested pRS303-loxP to generate pRS303-loxP-ATG9-3GFP. pRS303-loxP-Atg9-3mChe was generated by first excising the 3GFP region from pRS303loxP-ATG9-3GFP with *Bam*HI and *Sac*II, then adding three copies of mCherry using the 'cold fusion' kit from System Biosciences. Primers used to amplify mCherry were designed to have a specific sequence of homologous linkers so as to insert exactly three copies of mCherry joined by short flexible (gly-ser) linkers. The plasmid for CUP1 promoter-driven overexpression of Atg11 was pCuCVT9(414) (10). Plasmids AD-Atg11 and BDU-Atg9-N were also previously described (29).

The construction of the centromeric plasmids expressing *ATG* genes under their native promoters used for addition of these genes to the MKO strain is described in Table S1.

Strain generation

All strains are listed in Table 1. *RFP-APE1*::*LEU2*, *BFP-APE1*::*LEU2* and *mChe-APE1*::*TRP* strains were generated by the integration of *Cla*I-linearized pRS305-RFP-Ape1 (40), pRS305-BFP-Ape1, or *Avr*II-linearized pRS404-mChe-Ape1, respectively. *Stu*I was used to linearize pRS306-ATG9-3GFP (19), pRS406-ATG9-GFP and pRS406-TPI1p-ATG9-GFP (6) prior to integration. *ATG9-3GFP* and *ATG9-3mChe* (markerless) strains were generated by integration of *Xba*I-linearized pRS303-loxP-ATG9-3GFP or pRS303-loxP-ATG9-3mChe followed by removal of the *HIS3* marker by transformation with pSH47 (GAL-CRE overexpression plasmid with a *URA3* marker) and screening for clones which could no longer grow on -his or -ura plates after a few days of outgrowth.

*atg1*Δ::*LEU2*, *atg23*Δ and *atg27*Δ (markerless) strains were generated using the pUG set of knockout plasmids (41). Markers were removed from *atg23*Δ and *atg27*Δ by Cre expression as outlined above. *atg11*Δ::*HIS3*, *trs85*Δ::*TRP1* and *trs85*Δ::*KAN* strains and all *GAL1* overexpression strains were generated using the pFA6a series of plasmids (42). C-terminal m-Cherry-tagged secretory marker strains were generated using pFA6a-mCherry-V5-TRP1 or pFA6a-mCherry-V5-KanMX plasmids (6). *Trs85-yEGFP*::*KAN* was generated using plasmid pKT127(43).

Acknowledgments

This work was supported by NIH grants 1-F32-GM-101748-01 to S. K. B. and GM053396 to D. J. K. The authors declare that they have no conflicts of interest.

Supporting Information

Additional Supporting Information may be found in the online version of this article:

Table S1: Constructs used for the addition of *ATG* genes to the MKO strain

Movie S1: Atg9-3GFP in WT cells. Atg9-3GFP expressed under its native promoter as the only copy of Atg9 in otherwise WT cells (strain SKB170) imaged at 9 frames per second and played back at real speed.

Movie S2: Atg9-3GFP in MKO cells. Atg9-3GFP expressed under its native promoter in MKO cells (strain SKB138) imaged at 9 frames per second and played back at real speed.

References

1. Meijer WH, van der Klei IJ, Veenhuis M, Kiel JAKW. *ATG* genes involved in non-selective autophagy are conserved from yeast to man, but the selective Cvt and pexophagy pathways also require organism-specific genes. Autophagy 2007;3:106–116.
2. Mizushima N, Levine B, Cuervo AM, Klionsky DJ. Autophagy fights disease through cellular self-digestion. Nature 2008;451:1069–1075.
3. Seglen PO. Regulation of autophagic protein degradation in isolated liver cells. In: Glaumann H, Ballard FJ, editors. Lysosomes: Their Role in Protein Breakdown. London: Academ; 1987, pp. 371–414.
4. Baba M, Takeshige K, Baba N, Ohsumi Y. Ultrastructural analysis of the autophagic process in yeast: detection of autophagosomes and their characterization. J Cell Biol 1994;124:903–913.
5. Yen W-L, Shintani T, Nair U, Cao Y, Richardson BC, Li Z, Hughson FM, Baba M, Klionsky DJ. The conserved oligomeric Golgi complex is involved in double-membrane vesicle formation during autophagy. J Cell Biol 2010;188:101–114.
6. Mari M, Griffith J, Rieter E, Krishnappa L, Klionsky DJ, Reggiori F. An Atg9-containing compartment that functions in the early steps of autophagosome biogenesis. J Cell Biol 2010;190:1005–1022.
7. Wang K, Yang Z, Liu X, Mao K, Nair U, Klionsky DJ. Phosphatidylinositol 4-kinases are required for autophagic membrane trafficking. J Biol Chem 2012;287:37964–37972.
8. Yamamoto H, Kakuta S, Watanabe TM, Kitamura A, Sekito T, Kondo-Kakuta C, Ichikawa R, Kinjo M, Ohsumi Y. Atg9 vesicles are an important membrane source during early steps of autophagosome formation. J Cell Biol 2012;198:219–233.
9. Reggiori F, Tucker KA, Stromhaug PE, Klionsky DJ. The Atg1-Atg13 complex regulates Atg9 and Atg23 retrieval transport from the pre-autophagosomal structure. Dev Cell 2004;6:79–90.
10. Kim J, Kamada Y, Stromhaug PE, Guan J, Hefner-Gravink A, Baba M, Scott SV, Ohsumi Y, Dunn WA, Klionsky DJ. Cvt9/Gsa9 functions in sequestering selective cytosolic cargo destined for the vacuole. J Cell Biol 2001;153:381–396.
11. He C, Song H, Yorimitsu T, Monastyrska I, Yen W-L, Legakis JE, Klionsky DJ. Recruitment of Atg9 to the preautophagosomal structure by Atg11 is essential for selective autophagy in budding yeast. J Cell Biol 2006;175:925–935.

12. Sekito T, Kawamata T, Ichikawa R, Suzuki K, Ohsumi Y. Atg17 recruits Atg9 to organize the pre-autophagosomal structure. Genes Cells 2009;14:525–538.
13. Tucker KA, Reggiori F, Dunn WA, Klionsky DJ. Atg23 is essential for the cytoplasm to vacuole targeting pathway and efficient autophagy but not pexophagy. J Biol Chem 2003;278:48445–48452.
14. Legakis JE, Yen W-L, Klionsky DJ. A cycling protein complex required for selective autophagy. Autophagy 2007;3:422–432.
15. Yen W-L, Legakis JE, Nair U, Klionsky DJ. Atg27 Is required for autophagy-dependent cycling of Atg9. Mol Biol Cell 2007;18:581–593.
16. Nazarko TY, Huang J, Nicaud J-M, Klionsky DJ, Sibirny AA. Trs85 is required for macroautophagy, pexophagy and cytoplasm to vacuole targeting in *Yarrowia lipolytica* and *Saccharomyces cerevisiae*. Autophagy 2005;1:37–45.
17. Lynch-Day MA, Bhandari D, Menon S, Huang J, Cai H, Bartholomew CR, Brumell JH, Ferro-Novick S, Klionsky DJ. Trs85 directs a Ypt1 GEF, TRAPPIII, to the phagophore to promote autophagy. Proc Natl Acad Sci 2010;107:7811–7816.
18. Lipatova Z, Belogortseva N, Zhang XQ, Kim J, Taussig D, Segev N. Regulation of selective autophagy onset by a Ypt/Rab GTPase module. Proc Natl Acad Sci 2012;109:6981–6986.
19. Monastyrska I, He C, Geng J, Hoppe AD, Li Z, Klionsky DJ. Arp2 links autophagic machinery with the actin cytoskeleton. Mol Biol Cell 2008;19:1962–1975.
20. Backues SK, Klionsky DJ. Atg11: a Rab-dependent, coiled-coil membrane protein that acts as a tether for autophagy. Autophagy 2012;8:1275–1278.
21. Kakuta S, Yamamoto H, Negishi L, Kondo-Kakuta C, Hayashi N, Ohsumi Y. Atg9 vesicles recruit vesicle-tethering proteins Trs85 and Ypt1 to the autophagosome formation site. J Biol Chem 2012;287:44261–44269.
22. Cao Y, Cheong H, Song H, Klionsky DJ. In vivo reconstitution of autophagy in *Saccharomyces cerevisiae*. J Cell Biol 2008;182:703–713.
23. Cao Y, Nair U, Yasumura-Yorimitsu K, Klionsky DJ. A multiple *ATG* gene knockout strain for yeast two-hybrid analysis. Autophagy 2009;5:699–706.
24. Klionsky DJ, Cueva R, Yaver DS. Aminopeptidase I of *Saccharomyces cerevisiae* is localized to the vacuole independent of the secretory pathway. J Cell Biol 1992;119:287–299.
25. Geng J, Baba M, Nair U, Klionsky DJ. Quantitative analysis of autophagy-related protein stoichiometry by fluorescence microscopy. J Cell Biol 2008;182:129–140.
26. Nair U, Jotwani A, Geng J, Gammoh N, Richerson D, Yen W-L, Griffith J, Nag S, Wang K, Moss T, Baba M, McNew JA, Jiang X, Reggiori F, Melia TJ, et al. SNARE proteins are required for macroautophagy. Cell 2011;146:290–302.
27. Anitei M, Hoflack B. Exit from the trans-Golgi network: from molecules to mechanisms. Curr Opin Cell Biol 2011;23:443–451.
28. Bagnat M, Chang A, Simons K. Plasma membrane proton ATPase Pma1p requires raft association for surface delivery in yeast. Mol Biol Cell 2001;12:4129–4138.
29. Delacour D, Greb C, Koch A, Salomonsson E, Leffler H, Le Bivic A, Jacob R. Apical sorting by galectin-3-dependent glycoprotein clustering. Traffic 2007;8:379–388.
30. He C, Baba M, Cao Y, Klionsky DJ. Self-interaction is critical for Atg9 transport and function at the phagophore assembly site during autophagy. Mol Biol Cell 2008;19:5506–5516.
31. Young ARJ, Chan EYW, Hu XW, Köchl R, Crawshaw SG, High S, Hailey DW, Lippincott-Schwartz J, Tooze SA. Starvation and ULK1-dependent cycling of mammalian Atg9 between the TGN and endosomes. J Cell Sci 2006;119:3888–3900.
32. Ravikumar B, Moreau K, Jahreiss L, Puri C, Rubinsztein DC. Plasma membrane contributes to the formation of pre-autophagosomal structures. Nat Cell Biol 2010;12:747–757.
33. Orsi A, Razi M, Dooley HC, Robinson D, Weston AE, Collinson LM, Tooze SA. Dynamic and transient interactions of Atg9 with autophagosomes, but not membrane integration, are required for autophagy. Mol Biol Cell 2012;23:1860–1873.
34. Puri C, Renna M, Bento CF, Moreau K, Rubinsztein DC. Diverse autophagosome membrane sources coalesce in recycling endosomes. Cell 2013;154:1285–1299.
35. Popovic D, Dikic I. TBC1D5 and the AP2 complex regulate ATG9 trafficking and initiation of autophagy. EMBO Rep 2014;15:392–401.
36. Popovic D, Akutsu M, Novak I, Harper JW, Behrends C, Dikic I. Rab GTPase-activating proteins in autophagy: regulation of endocytic and autophagy pathways by direct binding to human ATG8 modifiers. Mol Cell Biol 2012;32:1733–1744.
37. Carpenter AE, Jones TR, Lamprecht MR, Clarke C, Kang IH, Friman O, Guertin DA, Chang JH, Lindquist RA, Moffat J, Golland P, Sabatini DM. CellProfiler: image analysis software for identifying and quantifying cell phenotypes. Genome Biol 2006;7:R100.
38. Schneider CA, Rasband WS, Eliceiri KW. NIH Image to ImageJ: 25 years of image analysis. Nat Methods 2012;9:671–675.
39. Noda T, Kim J, Huang W-P, Baba M, Tokunaga C, Ohsumi Y, Klionsky DJ. Apg9p/Cvt7p is an integral membrane protein required for transport vesicle formation in the Cvt and autophagy pathways. J Cell Biol 2000;148:465–480.
40. Strømhaug PE, Reggiori F, Guan J, Wang C-W, Klionsky DJ. Atg21 Is a phosphoinositide binding protein required for efficient lipidation and localization of Atg8 during uptake of aminopeptidase I by selective autophagy. Mol Biol Cell 2004;15:3553–3566.
41. Gueldener U, Heinisch J, Koehler GJ, Voss D, Hegemann JH. A second set of loxP marker cassettes for Cre-mediated multiple gene knockouts in budding yeast. Nucleic Acids Res 2002;30:e23.
42. Longtine MS, Mckenzie A III, Demarini DJ, Shah NG, Wach A, Brachat A, Philippsen P, Pringle JR. Additional modules for versatile and economical PCR-based gene deletion and modification in *Saccharomyces cerevisiae*. Yeast 1998;14:953–961.
43. Sheff MA, Thorn KS. Optimized cassettes for fluorescent protein tagging in *Saccharomyces cerevisiae*. Yeast 2004;21:661–670.
44. James P, Halladay J, Craig EA. Genomic libraries and a host strain designed for highly efficient two-hybrid selection in yeast. Genetics 1996;144:1425–1436.

45. Robinson JS, Klionsky DJ, Banta LM, Emr SD. Protein sorting in *Saccharomyces cerevisiae*: isolation of mutants defective in the delivery and processing of multiple vacuolar hydrolases. Mol Cell Biol 1988;8:4936–4948.

46. Kanki T, Wang K, Baba M, Bartholomew CR, Lynch-Day MA, Du Z, Geng J, Mao K, Yang Z, Yen W-L, Klionsky DJ. A genomic screen for yeast mutants defective in selective mitochondria autophagy. Mol Biol Cell 2009;20:4730–4738.